Mixture Coding and Segmentation in the Anterior Piriform Cortex

Sapir Penker, Tamar Licht, Katharina T. Hofer and Dan Rokni*

Department of Medical Neurobiology, School of Medicine and IMRIC, The Hebrew University of Jerusalem, Jerusalem, Israel

Coding of odorous stimuli has been mostly studied using single isolated stimuli. However, a single sniff of air in a natural environment is likely to introduce airborne chemicals emitted by multiple objects into the nose. The olfactory system is therefore faced with the task of segmenting odor mixtures to identify objects in the presence of rich and often unpredictable backgrounds. The piriform cortex is thought to be the site of object recognition and scene segmentation, yet the nature of its responses to odorant mixtures is largely unknown. In this study, we asked two related questions. (1) How are mixtures represented in the piriform cortex? And (2) Can the identity of individual mixture components be read out from mixture representations in the piriform cortex? To answer these questions, we recorded single unit activity in the piriform cortex of naïve mice while sequentially presenting single odorants and their mixtures. We find that a normalization model explains mixture responses well, both at the single neuron, and at the population level. Additionally, we show that mixture components can be identified from piriform cortical activity by pooling responses of a small population of neurons—in many cases a single neuron is sufficient. These results indicate that piriform cortical representations are well suited to perform figure-background segmentation without the need for learning.

Keywords: olfaction, smell, normalization, figure-background, odor

INTRODUCTION

The odorants emitted by different objects in the environment mix in the air before reaching the nose. Each of these objects in itself will typically emit tens to thousands of odorants that become its olfactory signature. Natural inputs into the olfactory system are therefore rich odorant mixtures that require segmentation in order for useful information to be extracted. The difficulty of mixture segmentation arises from the overlapping representations of odorants by olfactory sensory neurons (Malnic et al., 1999; Rubin and Katz, 1999; Araneda et al., 2000; Kajiya et al., 2001; Abaffy et al., 2006; Grosmaitre et al., 2009; Soucy et al., 2009). Similar to the auditory system (and unlike the visual system), a single sensory neuron may be simultaneously activated by multiple odorants (Brungart et al., 2001; McDermott, 2009). Behavioral testing has indeed shown that increased overlap in odorant representations is related to increased difficulty of scene segmentation (Rokni et al., 2014).

The mechanisms for scene segmentation are not well understood. Piriform cortex, being the first brain station that combines inputs from multiple receptor channels, is a primary candidate for performing this task (Davison and Ehlers, 2011; Ghosh et al., 2011; Sosulski et al., 2011; Haddad et al., 2013). Several factors have been suggested to contribute. First, if objects are dispersed in space, plume dynamics may provide temporal separation between

objects (Hopfield, 1995; Brody and Hopfield, 2003; Wilson, 2003; Kadohisa and Wilson, 2006a; Linster et al., 2007; Szyszka et al., 2012; Vinograd et al., 2017; Erskine et al., 2019). Second, readout of mixture components can be achieved by properly combining inputs form multiple receptor channels (Mathis et al., 2016; Singh et al., 2019). And third, feedback projections within the olfactory system may provide a flexible readout for specific mixture components (Li and Hertz, 2000; Grabska-Barwińska et al., 2017; Singh et al., 2019).

Currently a limiting factor in understanding mixture segmentation, is our limited knowledge about mixture coding. Understanding how odor mixtures are represented in the piriform cortex is a prerequisite for understanding mixture segmentation. Ultimately we would want to be able to predict responses to mixtures based on the responses to single components. Several studies have reported sublinear mixture responses in olfactory cortex, thereby limiting the possible response space, however, they have not provided models to predict mixture responses (Lei et al., 2006; Yoshida and Mori, 2007; Stettler and Axel, 2009). Sublinearlity of mixture responses is probably inherited to some extent from the olfactory epithelium (Kurahashi et al., 1994; Duchamp-Viret et al., 2003; Oka et al., 2004; Takeuchi et al., 2009; Xu et al., 2020; Zak et al., 2020), as well as from the olfactory bulb where cross odorant inhibition may contribute (Yokoi et al., 1995; Urban, 2002; Aungst et al., 2003; McGann et al., 2005; Arevian et al., 2008; Fantana et al., 2008). The piriform cortex integrates these non-linear odor representations from the olfactory bulb and utilizes local recurrent circuitry to generate representations that presumably support segmentation (Poo and Isaacson, 2009, 2011; Franks et al., 2011; Miura et al., 2012; Suzuki and Bekkers, 2012; Roland et al., 2017; Bolding and Franks, 2018). Importantly, piriform cortex is also expected to contribute to sublinear summation of mixture components due to local inhibitory circuits. These circuits have been shown to normalize responses to increasing concentrations of odors (Bolding and Franks, 2018; Stern et al., 2018). Whether increasing stimulus intensity by increasing concentration or by adding more odorants produces equivalent normalization is unknown. Piriform cortex is typically divided into anterior and posterior regions. The anterior piriform cortex receives more afferent inputs from the olfactory bulb and less associational inputs than the posterior piriform cortex (Hagiwara et al., 2012; Giessel and Datta, 2014). This connectivity difference suggests that the anterior piriform cortex may reflect the input itself with greater acuity rather than its learned associations (Wilson and Sullivan, 2011).

Several questions remain unanswered about mixture representations. First, how do cortical mixture representations relate to the representations of their constituent odorants? In other words, how can one predict cortical responses to mixtures from the responses to single components? And second, how is information about the individual mixture components represented in the piriform cortex and how can it be read by down-stream regions?

To answer these questions, we systematically characterized mixture representations in the anterior piriform cortex and analyzed their ability to convey information about individual mixture components, at both the single neuron, and population levels. We focus our analysis on the anterior piriform cortex because of its tighter link to the stimulus.

MATERIALS AND METHODS

All experimental procedures were performed using approved protocols in accordance with institutional (Hebrew University IACUC) and national guidelines.

Data Acquisition

Young adult male c57bl6 mice (10–14 weeks old, Envigo) were anesthetized (Ketamine/Medetomidine 75 and 1 mg/kg, respectively), and were restrained in a stereotaxic device (Model 940, David Kopf Instruments). The skin was removed from the scalp and a small craniotomy was made over the anterior piriform cortex (1.5 mm anterior and 2.8 mm lateral to bregma). A metal plate was attached to the skull with dental acrylic and was used to hold mice at the electrophysiological rig. Normal body temperature (37 C) was maintained with a heating pad (Harvard Apparatus). A single tungsten electrode (A-M systems, 10–12 MOhm) was lowered into the piriform cortex with a micromanipulator (Sutter Instruments). Signals from the electrode were band pass filtered (300–5,000 Hz), amplified (X1000, A-M systems 1800), and sampled at 20 KHz and digitized with 16-bit precision (National Instruments PCIe-6351). All analog signals were displayed and saved for offline analysis using custom-made software in LabVIEW (National Instruments). Injections of a TRITC-labeled 10Kd dextran (500 nL, Molecular probes cat#D1817, 10 mg/ml) were used to verify piriform cortical targeting.

Odors were presented using a custom-made, computer-controlled, odor presentation machine that maintains constant flow and allows mixing of odors without mutual dilution (Rokni et al., 2014). The following 8 odorants were used (all from Sigma Aldrich, CAS numbers in parentheses): (1) isobutyl propionate (540-42-1), (2) 2-ethyl hexanal (123-05-7), (3) ethyl valerate (539-82-2), (4) propyl acetate (109-60-4), (5) isoamyl tiglate (41,519-18-0), (6) phenethyl tiglate (55,719-85-2), (7) citral (5,392-40-5), (8) ethyl propionate (105-37-3). All odorants were diluted to 10% in diethyl phthalate (84-66-2), and then further diluted eightfold in air. Odors were presented into a mask that fit the mouse's snout at a rate of 1 l/min and were cleared from the mask by vacuum that was set to create an outward flow of 1 l/min (**Figure 1A**). A third port of the mask was connected to a mass flow sensor (Honeywell AWM3300) to monitor respiration. For each recording session, a set of 4 odorants was chosen (initially randomly and later fixed to odorants 1, 3, 5, and 7). All 15 combinations of these 4 odorants were then presented with randomized order (typically repeating ~30 times each). Odors were presented for 1.5 s with an inter-trial interval of 20 s.

Data Analysis

Action potentials were detected offline using custom-written code in Matlab, and were then sorted using MClust (David Redish). Only units that had less than 1 in 1,000 spikes to
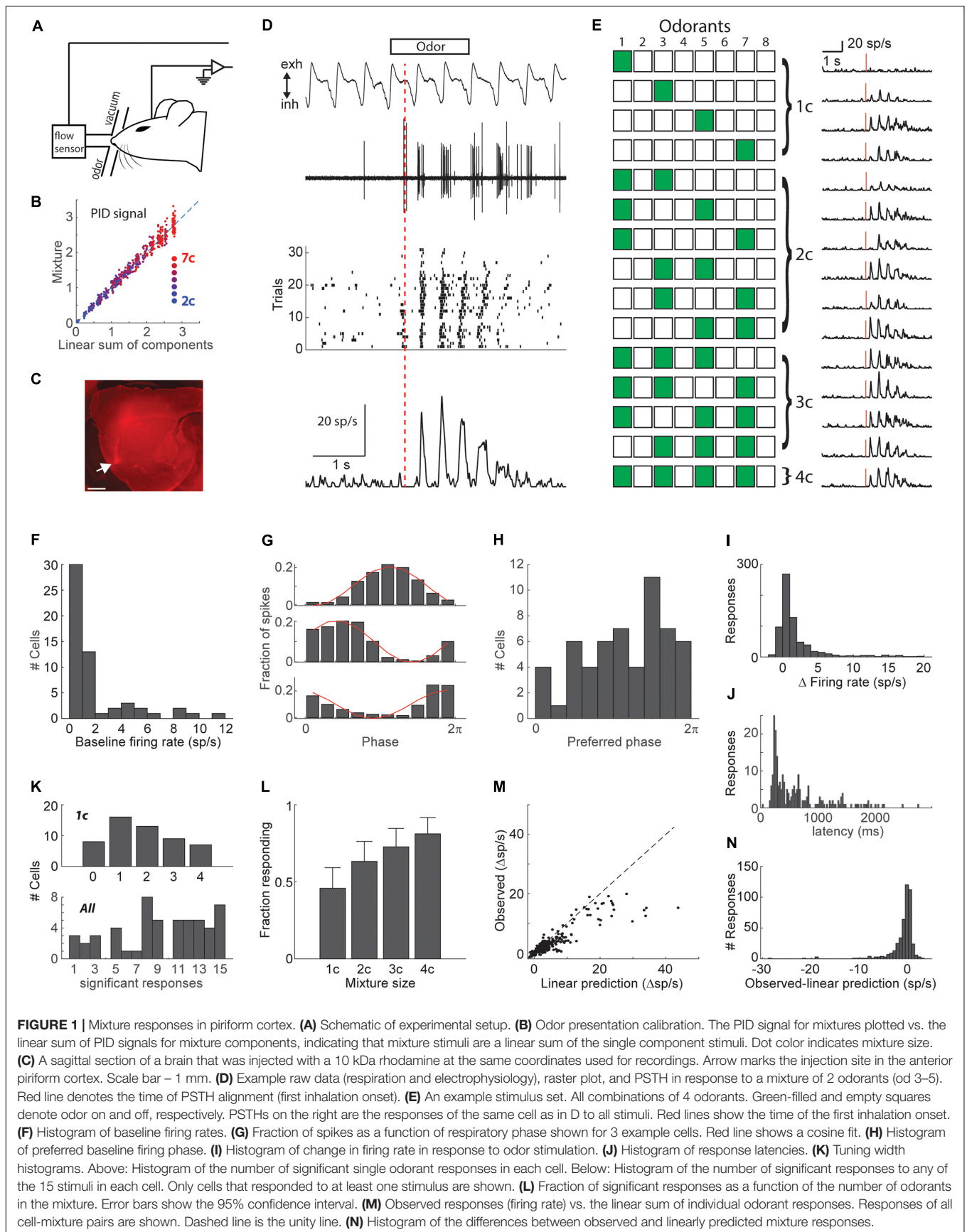
FIGURE 1 | Mixture responses in piriform cortex. **(A)** Schematic of experimental setup. **(B)** Odor presentation calibration. The PID signal for mixtures plotted vs. the linear sum of PID signals for mixture components, indicating that mixture stimuli are a linear sum of the single component stimuli. Dot color indicates mixture size. **(C)** A sagittal section of a brain that was injected with a 10 kDa rhodamine at the same coordinates used for recordings. Arrow marks the injection site in the anterior piriform cortex. Scale bar – 1 mm. **(D)** Example raw data (respiration and electrophysiology), raster plot, and PSTH in response to a mixture of 2 odorants (od 3–5). Red line denotes the time of PSTH alignment (first inhalation onset). **(E)** An example stimulus set. All combinations of 4 odorants. Green-filled and empty squares denote odor on and off, respectively. PSTHs on the right are the responses of the same cell as in D to all stimuli. Red lines show the time of the first inhalation onset. **(F)** Histogram of baseline firing rates. **(G)** Fraction of spikes as a function of respiratory phase shown for 3 example cells. Red line shows a cosine fit. **(H)** Histogram of preferred baseline firing phase. **(I)** Histogram of change in firing rate in response to odor stimulation. **(J)** Histogram of response latencies. **(K)** Tuning width histograms. Above: Histogram of the number of significant single odorant responses in each cell. Below: Histogram of the number of significant responses to any of the 15 stimuli in each cell. Only cells that responded to at least one stimulus are shown. **(L)** Fraction of significant responses as a function of the number of odorants in the mixture. Error bars show the 95% confidence interval. **(M)** Observed responses (firing rate) vs. the linear sum of individual odorant responses. Responses of all cell-mixture pairs are shown. Dashed line is the unity line. **(N)** Histogram of the differences between observed and linearly predicted mixture responses.

have occurred within a 3 ms refractory period were considered as single units and further analyzed. Respiratory signals were low-pass filtered with a moving average window of 250 ms. Inhalation onsets were defined as zero crossings with negative slope. All neural responses were aligned to the first inhalation onset following odor onset. PSTHs were generated with 1 ms bins and filtered with a 50 ms window Gaussian moving average. Response significance was tested by comparing spike rates during a 3 s response period to the spike rates in a 3 s period with no odor, using the Wilcoxon ranksum test with a threshold p-value of 0.01. Response latency was defined as the first bin in which firing rate deviated from an equivalent non-odor time bin with a $p < 0.01$ using the Kolmogorov-Smirnov test. All responses are shown as baseline-subtracted spike rates. To fit normalization models, data was fit to equation 1 using the lsqcurvefit function in Matlab. Fit quality was assessed with the coefficient of determination (R^2).

Receiver operating characteristic (ROC) analysis was performed using the perfcurve function in Matlab. For each neuron, ROC analysis was performed separately to test the detectability of each odorant. The reported performance of each neuron is the best across the 4 odorants. The performance reported for each odorant is the best across all neurons. Shuffled controls were created by shuffling the stimulus labels for all neurons and obtaining a distribution of 224 auROC values (4 odorants X 56 neurons). Performance is reported as above control if the auROC was above all shuffled controls.

For population analysis, we generated a pseudo-population by pooling neurons from different experiments in which we used the same 4 odorants (odorants 1, 3, 5, and 7). Principal component analysis was performed after normalizing each neuron's responses to its standard deviation. For modeled mixture responses we created modeled PSTHs for each neuron. The linear, mean, and max modeled PSTHs were created by taking the linear sum, mean, and maximum of the individual component responses, respectively. The normalization model PSTHs were created by simultaneously fitting a pair of parameters to all mixture responses of a neuron (Eq. 1).
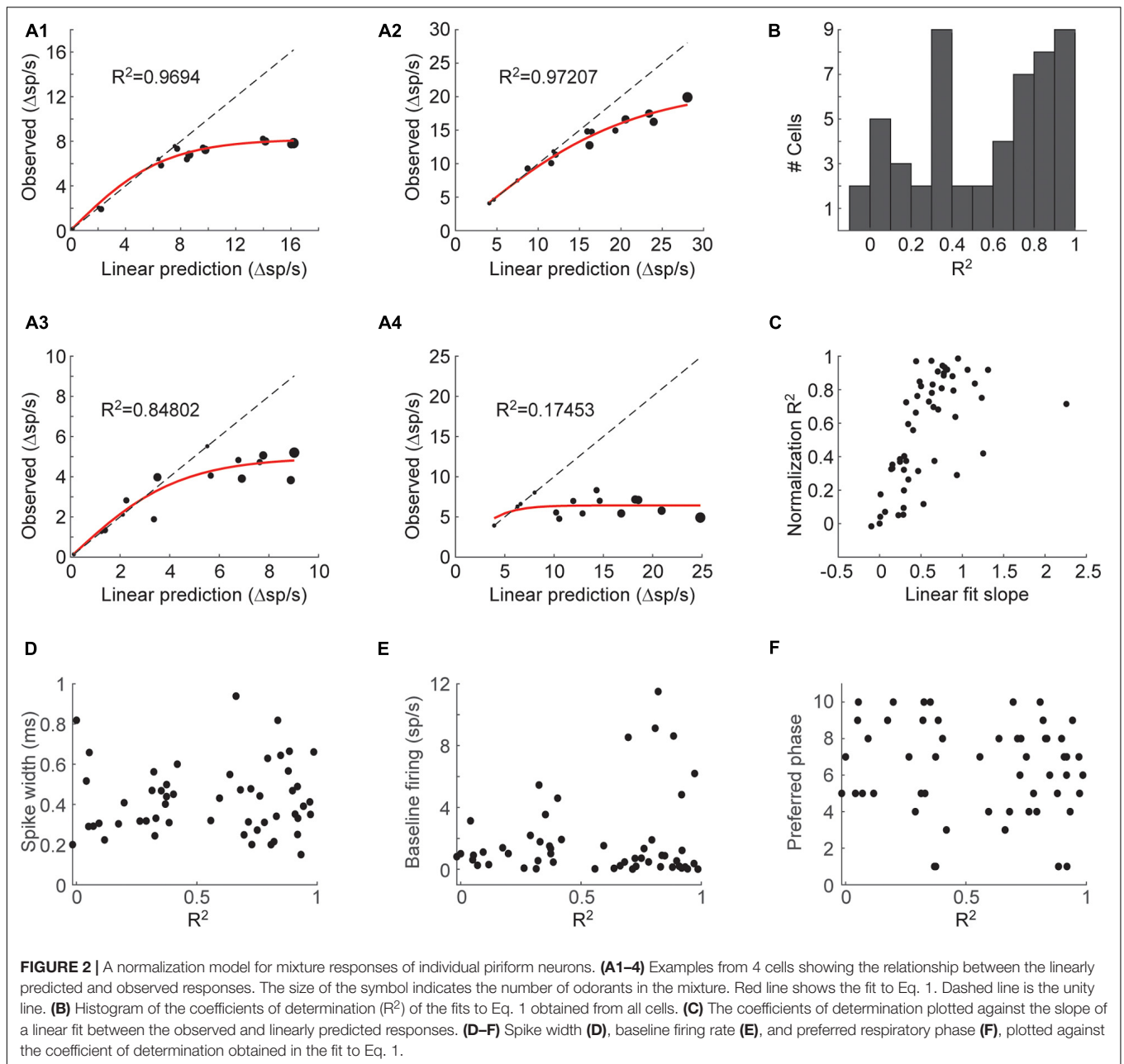
Linear classifiers were realized as logistic regressions and were fit using the fitclinear function in Matlab. The cost function for the classifier is $\ell[y, f(x)] = \log\{1 + \exp[-yf(x)]\}$, where y is the data and f(x) if the fit. The fit minimizes this cost function. Classifiers were cross-validated by creating a test set that was not used for training. Each test set included one randomly selected response from each neuron to each of the 15 odor combinations. A training set that did not include the testing trials was then generated by randomly selecting trials from each neuron for each odor combination. The training set included 1,000 trials of each of the 15 stimuli for most analyses. The reported performance for the classifiers is the mean over 100 iterations. For assessing the effect of population size on classification accuracy, we gradually removed inputs from the classifier by sequentially removing the neuron with the minimal absolute weight. For the analysis of temporal resolution, time bins from all neurons were concatenated in each trial and the training set was increased to 10,000 trials for each stimulus.

RESULTS

We recorded the responses of single neurons in the anterior piriform cortex of naïve anesthetized mice, to all possible combinations of 4 odorants (4 single odorants, 6 pairs, 4 triplets, 1 mix of 4, **Figures 1A–E**). Various sets of 4 odorants were used. Because the isolation of single-unit activity is critical for the following analysis, we recorded neural activity using single tungsten electrodes which provide a much higher signal to noise ratio than most multi-channel systems and allow better separation of single-unit spikes. We recorded from 56 well-isolated neurons from 27 mice. 53 neurons responded significantly to at least one of the 15 stimuli (single odorant or mixture). Odors were presented using a machine that allows mixing of odors without mutual dilution, into a mask that fit the mouse snout and were cleared with constant negative pressure (**Figures 1A,B**). The mask was connected to a mass flow sensor for continuous monitoring of respiration. Dye injections in the recording coordinates (1.5 mm anterior and 2.8 mm lateral to Bregma, 4.5 mm ventral), verified targeting of anterior piriform cortex (**Figure 1C**). All odor responses were aligned to the first inhalation onset following odor valve opening, and typically showed a strong locking to respiration (**Figures 1D,E**).

The basal firing of cortical neurons was typically very low (1.9 ± 0.05 Hz, mean ± SEM, **Figure 1F**), and both basal firing and odor responses were typically strongly modulated by respiration (**Figures 1E,G,H**). Odor responses were predominantly positive (increases in firing rate) with only 18% showing mild decreases in firing rate (**Figure 1I**). This however may be an underestimate of inhibitory inputs as most neurons had a basal firing rate of less than 1 spike per second, rendering our analysis less sensitive to inhibition. Response latency showed a wide range starting from 150 ms (**Figure 1J**). Of the responding neurons, most responded significantly to more than one of the individual odorants (**Figure 1K**). We first asked whether adding odorants to a mixture increases overall responses in the piriform cortex. Analyzing response statistics across all responsive neurons, we found that the fraction of significant responses ($p < 0.01$) was positively correlated with the number of mixture components ($r = 0.98$, $p = 0.017$, **Figure 1L**). The simplest model for response integration is a linear model in which a neuron's response to a mixture is equal to the sum of its responses to the mixture components. To test for linearity of odorant integration, we compared mixture responses of all neurons to the linear sum of the responses to individual mixture components. Most mixture responses were below the linear prediction (**Figures 1M,N**). These analyses show that in agreement with previous studies, the vast majority of piriform cortical responses to odorant mixtures increase with added mixture components and that this increase is sublinear (Lei et al., 2006; Yoshida and Mori, 2007; Stettler and Axel, 2009).

We next asked whether there is any consistent shape to the relationship between the linear predictions and the observed responses. We first treated responses as the mean firing rate within a 3 s response period. We fitted mixture responses with a logistic function to describe response normalization, similarly

FIGURE 2 | A normalization model for mixture responses of individual piriform neurons. **(A1–4)** Examples from 4 cells showing the relationship between the linearly predicted and observed responses. The size of the symbol indicates the number of odorants in the mixture. Red line shows the fit to Eq. 1. Dashed line is the unity line. **(B)** Histogram of the coefficients of determination (R^2) of the fits to Eq. 1 obtained from all cells. **(C)** The coefficients of determination plotted against the slope of a linear fit between the observed and linearly predicted responses. **(D–F)** Spike width **(D)**, baseline firing rate **(E)**, and preferred respiratory phase **(F)**, plotted against the coefficient of determination obtained in the fit to Eq. 1.

to fits used to describe mixture responses in olfactory sensory neurons (Mathis et al., 2016):

$$R = Rmax\left(\frac{2}{1 + e^{-s \cdot LP}} - 1\right) \qquad (1)$$

In this model, R is the neuron's response to a mixture, LP is the linear sum of the individual component responses, $Rmax$ is the neuron's maximal response, and s is a parameter that sets the initial slope of the function (at $LP = 0$). $Rmax$ and s are the two fitted parameters. We found that this model explains mixture responses well for most neurons (**Figures 2A1–3**). Some neurons however, could not be properly

fit (**Figure 2A4**). The normalization model could account for most of the variance (R^2 above 0.5) in 30/53 (57%) of the cells (**Figure 2B**). The neurons that could not be well explained with this model (low R^2) showed little increase in their responses as mixture components were added as assessed by the slope of a linear fit between the linear prediction and the observed responses (**Figure 2C**). Whether these neurons represent a separate neuronal subtype is unclear, yet the quality of the normalization fit was not correlated with spike waveform, basal firing rate or preferred respiratory phase of firing (**Figures 2D–F**). These results indicate that mixture responses of individual piriform neurons can often be explained by a simple normalization model.

To assess how the variable fit quality across cells affects population coding in piriform cortex, and how these responses evolve in time, we analyzed response trajectories of 37 neurons that were recorded using the same odorant set (odors 1, 3, 5, and 7). We used principal component analysis to visualize response trajectories (**Figure 3**). Mixture responses typically occupied the space between the component responses (**Figure 3A**). To test how well the normalization model explains population responses, we created normalized PSTHs for each mixture and projected them onto PCA space (**Figure 3B**). Normalized PSTHs were created by simultaneously fitting a single pair of parameters to all mixture responses of each neuron. We tested 3 other models for comparison: (1) a linear model in which the predicted mixture response is the sum of the component responses. (2) a mean model in which the mixture response is predicted to be the average of the component responses. And (3) a max model in which the predicted mixture response is the maximum of the component responses (**Figures 3B,C**). We compared the errors produced by the four models by measuring the Euclidean distance between the modeled PSTHs and the actual observed responses. Overall the normalization model was the most accurate with the lowest distance for 9 out of the 11 mixtures (**Figures 3G,H**, $p = 0.005$ vs. mean, $p = 0.001$ vs. max, $p = 0.001$ vs. linear, Wilcoxon signed rank test). To assess the accuracy of the normalization model, we compared its errors to the distances between the 15 different presented stimuli. The model errors were significantly lower than the inter-stimulus distances, despite the fact that our stimuli have many shared odorants (**Figure 3I**). These results indicate that population coding of mixtures in piriform cortex can be explained by a normalization model.

One of the suggested tasks that the piriform cortex is presumed to solve is figure-background segmentation. It was recently suggested that individual piriform neurons may be able to detect target odors in a background-invariant manner by pooling inputs from multiple glomeruli (Mathis et al., 2016; Grabska-Barwińska et al., 2017; Singh et al., 2019). We therefore asked whether the presence of individual odorants in mixtures can be extracted from the activity of individual piriform neurons. We used receiver operator characteristic (ROC) analysis to test whether the responses to mixtures that contain a specific target odorant are discriminable from responses to mixtures that do not contain the target odorant (**Figure 4**; Green and Swets, 1966). For each neuron, we assessed discriminability for all 4 odorants in the experiment and used the best discriminated odorant as target. We quantified discriminability with the area under the ROC curve (auROC, **Figures 4A,B**). Many neurons yielded high levels of discriminability with 54/56 (96%) neurons performing better than shuffled-labels controls, and 11/56 (20%) cells having an auROC of above 0.8. The discriminability for each odorant based on its single best neuron ranged from auROC of 57–99.7 and averaged at 79 (**Figure 4C**). Mice detect target odorants from background mixtures in about 500 ms (Rokni et al., 2014). We therefore analyzed how single neuron target detection is affected by the time window over which responses are integrated. Responses integrated within a window of less than 200 ms from stimulus onset were not informative about

target odorants and the auROC curve plateaued for most neurons between 800 and 1,600 ms (**Figure 4D**). The longer integration windows are presumably more informative about target odorants due to increased spike counts and signal to noise ratio, but they may also be more informative because they cover the right epoch in which action potentials carry the most information about the presence of the target odorant. To analyze for the latter, we repeated the ROC analysis with 200 ms windows that were shifted in time (**Figure 4E**). 12/56 neurons had at least one 200 ms epoch for which the auROC was above 0.8. The auROC as a function of time for these 12 neurons was highly correlated with the shape of their PSTHs in response to the target odorants. These analyses indicate that single piriform neurons are highly informative about the presence of a target odorant within a mixture, and that detection can be performed in time scales that match previous behavioral measurements. Nevertheless, since olfactory responses are often sharpened when analyzed with respect to sniff phase rather than absolute time (Shusterman et al., 2011; Ackels et al., 2020), we repeated the ROC analysis using sniff warped trials. Sniff warped and sniff aligned analyses obtained almost identical results due to the low variability of sniff rates in the anesthetized condition (**Supplementary Figure S1**).

Despite the overall good performance of target odorant detection form the activity of single neurons, some odorants could not be accurately detected (see odors 3 and 7 in **Figure 4C**). We therefore next analyzed the ability to detect target odorants from the activity of neuronal populations. We pooled data from all cells stimulated with a specific set of 4 odorants (odorants 1, 3, 5, and 7, 37 cells) to create a pseudo-population. We then trained linear classifiers (realized as logistic regressions) to classify trials according to the presence of each individual odorant. Classifiers were cross-validated by constructing a test set that included a single response from each neuron to each of the 15 odor combinations. Test set responses were not included in the training set. The mean classification accuracy across target odorants was 88% correct (99% for odorant 1, 88% for odorant 3, 86% for odorant 5, and 78% for odorant 7), showing a significant improvement for the odorants that were not well detected with single neurons. The performance of the classifiers typically decreased for richer mixtures, starting from an average performance of $94 \pm 2\%$ for single odorants and decreasing to $82 \pm 6\%$ for mixtures with 4 components (**Figure 5A**). To assess the number of neurons required to detect individual odorants from mixtures, we trained classifiers using sub-populations (**Figure 5B**). We started with the entire population and gradually removed the neuron with the minimal absolute weight. On average across odors, 6 neurons were sufficient to reach a performance level above 90% of the level achieved with the entire population (1 neuron for odorant 1, 8 for odorant 2, 7 for odorant 3, and 6 for odorant 4). We next asked whether target odorants can be detected within behavioral time scales. To that end, we analyzed how classifier performance depends on the response integration time (**Figure 5C**). Classifier performance degraded only for one target odorant when decreasing the integration time from 3 to 1 s, but degraded sharply for all target odorants when decreasing the integration window below
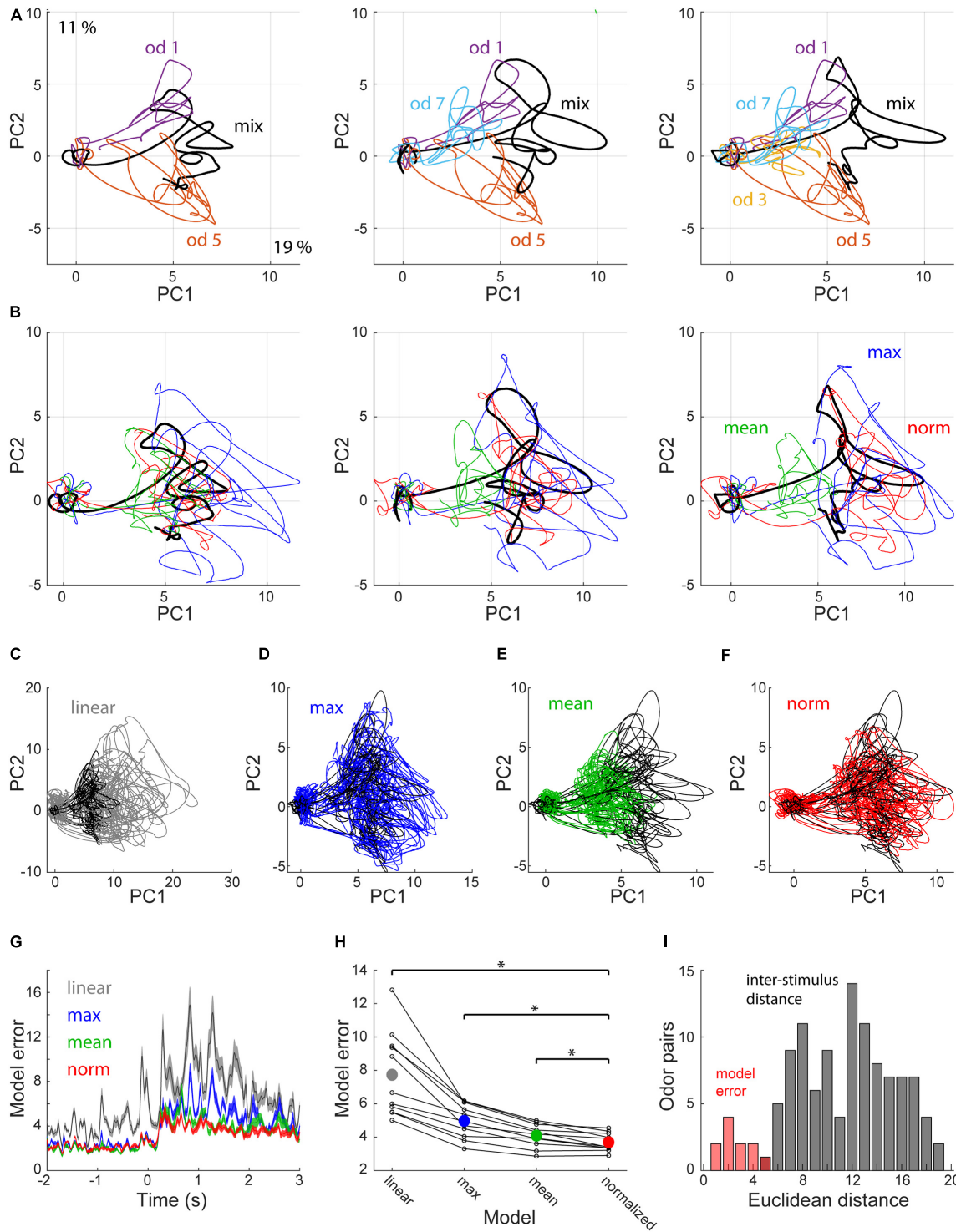
FIGURE 3 | Population coding of mixture responses. (A) Projections of single odorant (colored) and respective mixture responses (black) onto the first 2 principal components explaining 19 and 11 percent of the variance, respectively. Shown are examples for mixtures of 2, 3, and 4 odorants. (B) PCA projections of the same mixture responses as in (A) (black) and 3 corresponding predicted responses. Blue—max, Green—mean, Red—normalization. (C–F) PCA projections of all 11 mixture responses (black) and their corresponding predicted responses (colored). (C) Linear prediction. (D) Max prediction. (E) Mean prediction. (F) Normalization prediction. (G) Model errors, calculated as the Euclidean distance between the observed and predicted mixture responses as a function of time. Colors as in (B–F) shown are mean ± SEM. (H) Mean model error distance during odor presentation for all model-mixture pairs. Dots representing the same mixture are connected with lines. Colored dots show the mean. Asterisks reflect statistical significance ($p < 0.01$). (I) Normalization model error for the 11 mixtures (red), and all pairwise inter-stimulus distances (gray). *Denote $p < 0.01$ Wilcoxon signed rank test.
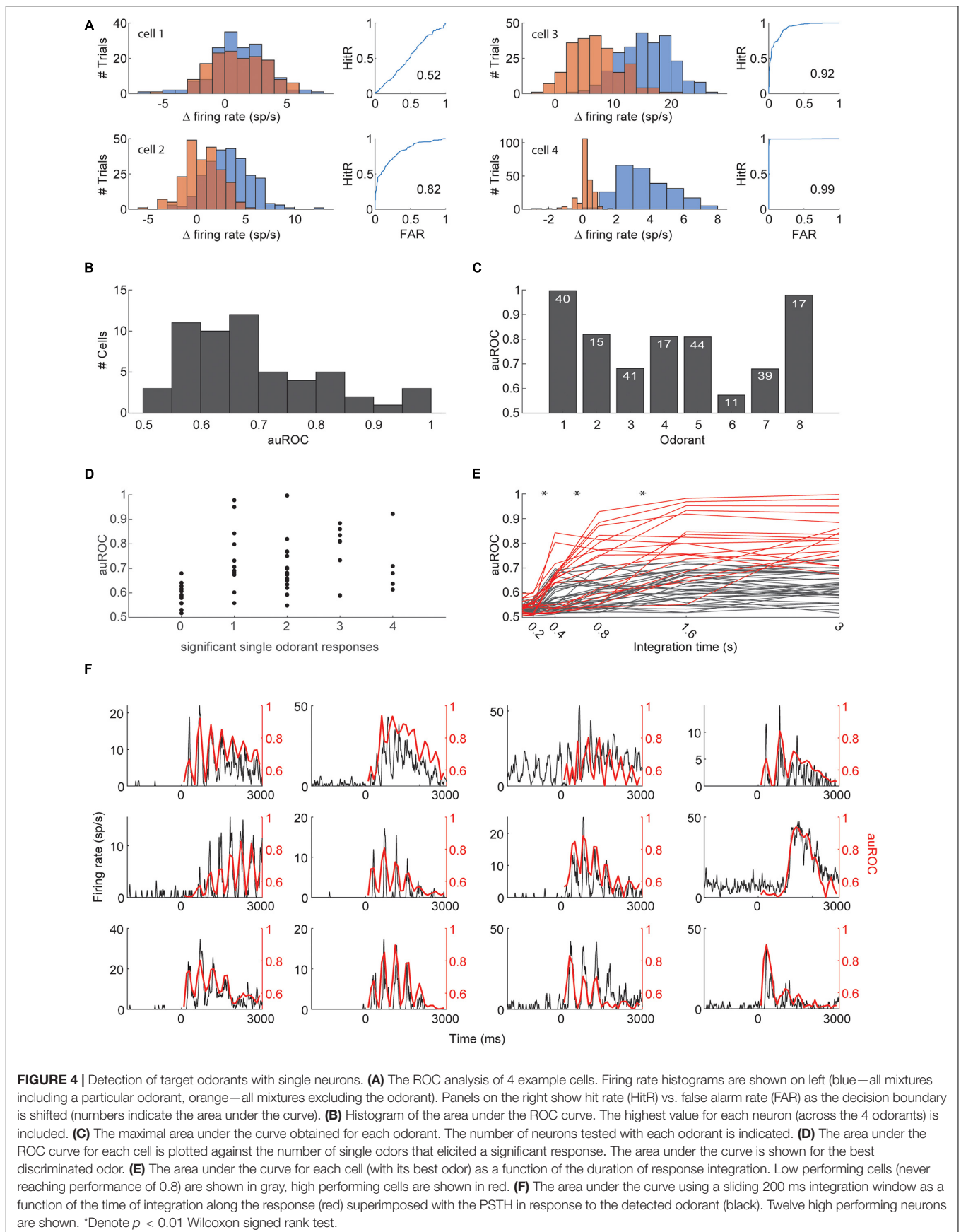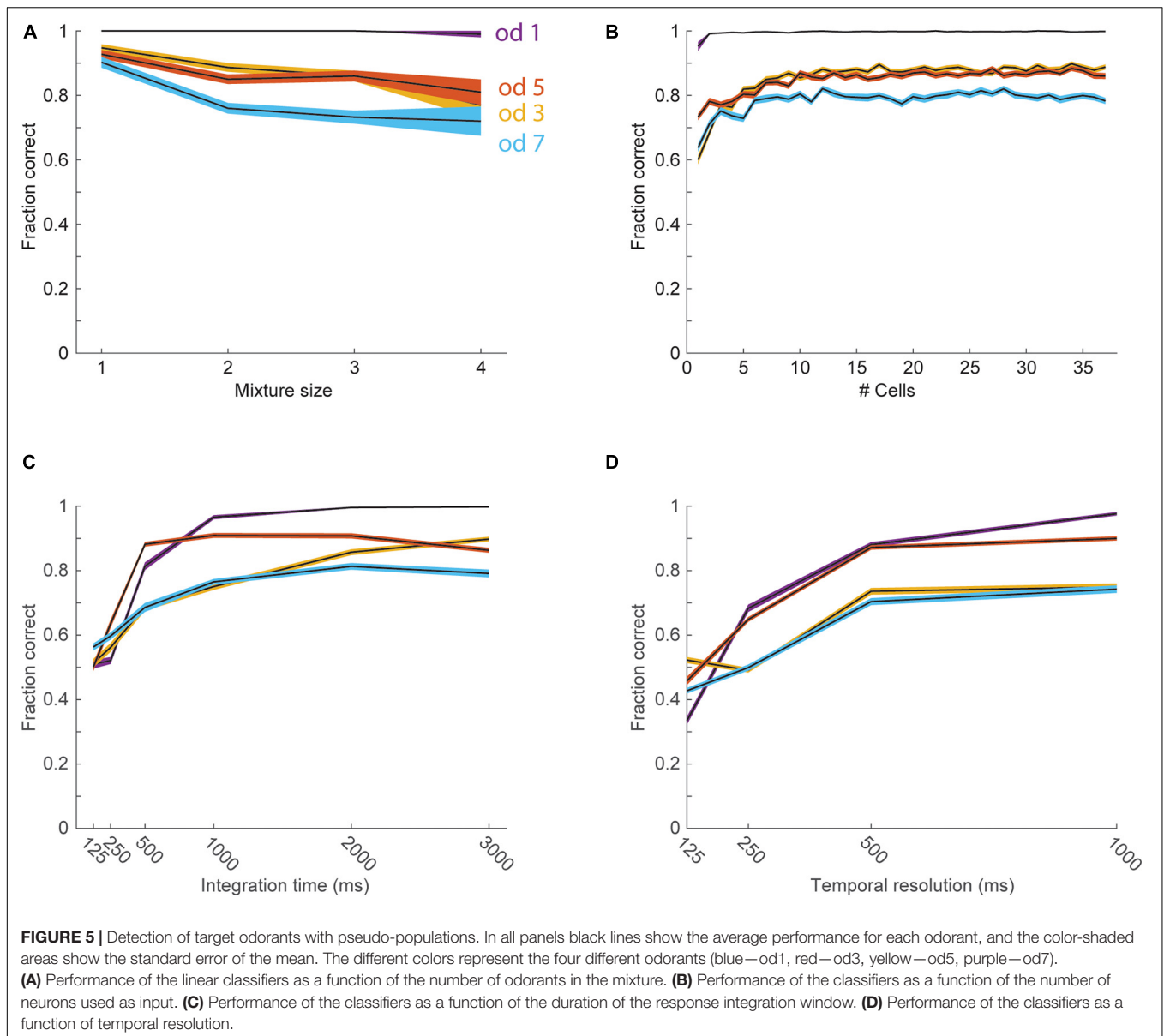
FIGURE 4 | Detection of target odorants with single neurons. **(A)** The ROC analysis of 4 example cells. Firing rate histograms are shown on left (blue—all mixtures including a particular odorant, orange—all mixtures excluding the odorant). Panels on the right show hit rate (HitR) vs. false alarm rate (FAR) as the decision boundary is shifted (numbers indicate the area under the curve). **(B)** Histogram of the area under the ROC curve. The highest value for each neuron (across the 4 odorants) is included. **(C)** The maximal area under the curve obtained for each odorant. The number of neurons tested with each odorant is indicated. **(D)** The area under the ROC curve for each cell is plotted against the number of single odors that elicited a significant response. The area under the curve is shown for the best discriminated odor. **(E)** The area under the curve for each cell (with its best odor) as a function of the duration of response integration. Low performing cells (never reaching performance of 0.8) are shown in gray, high performing cells are shown in red. **(F)** The area under the curve using a sliding 200 ms integration window as a function of the time of integration along the response (red) superimposed with the PSTH in response to the detected odorant (black). Twelve high performing neurons are shown. *Denote $p < 0.01$ Wilcoxon signed rank test.

FIGURE 5 | Detection of target odorants with pseudo-populations. In all panels black lines show the average performance for each odorant, and the color-shaded areas show the standard error of the mean. The different colors represent the four different odorants (blue—od1, red—od3, yellow—od5, purple—od7). **(A)** Performance of the linear classifiers as a function of the number of odorants in the mixture. **(B)** Performance of the classifiers as a function of the number of neurons used as input. **(C)** Performance of the classifiers as a function of the duration of the response integration window. **(D)** Performance of the classifiers as a function of temporal resolution.

500 ms. The average performance across odors with 500 ms integration time was $77 \pm 5\%$, indicating that much of the information for classification is available within the behavioral time limits. Lastly, we tested whether spike timing carries any information beyond what is carried by the mean firing rates. We trained classifiers with temporal inputs at varying temporal resolution (**Figure 5D**). Decreasing time bins below 500 ms yielded over-fitted models that performed badly on test trials. Even when the total response duration was lowered to 1 s and the number of training trials was increased 100-fold, time bins below 500 ms yielded over-fitted models. As with the ROC analysis, we repeated the classifier analysis using sniff phase instead of time and obtained very similar results (**Supplementary Figure S1**). This indicates that the anterior piriform cortex uses a rate code to convey information about the presence of target odors

embedded in background mixtures. Together, these analyses show that the detection of target odorants against background mixtures can be reliably achieved with a small number of piriform neurons.

DISCUSSION

We recorded from single neurons in the anterior piriform cortex of naïve anesthetized mice and describe their responses to odorant mixtures. We used receiver operator characteristic (ROC) analysis, and linear classifiers to describe the availability of information regarding mixture components in single neuron, and population activity, respectively. Our main findings are that (i) piriform responses can be described with a normalization

model that relates mixture responses to the linear sum of individual component responses, and previous analyses of mixture representations in the piriform cortex have found that sub-linear summation of odorant responses is the common case, although examples of supra-linear summation have also been demonstrated (Yoshida and Mori, 2007; Stettler and Axel, 2009). Similar variability in odorant summation has also been found in the anterior olfactory nucleus (Lei et al., 2006). Our analysis shows that combining multiple mixture responses of individual neurons uncovers a mathematical relationship between them. The normalization model may explain some of the variability in previous studies as responses far below the saturation level (R_{max} in eq. 1) may appear linear while greater responses will be sublinear. Normalization has been found in many cortical regions and has been proposed as a canonical computation performed by cortical circuits that allows them to encode variables monotonically without saturating (Carandini and Heeger, 2012). Our finding of mixture response normalization is in line with studies that demonstrated normalization of responses to increasing concentrations of odorants (Bolding and Franks, 2017, 2018; Stern et al., 2018). Several mechanisms may contribute to the sublinear summation of odorant responses. These include interactions between odorants at the olfactory epithelium (Kurahashi et al., 1994; Duchamp-Viret et al., 2003; Oka et al., 2004; Grossman et al., 2008; Takeuchi et al., 2009; Reddy et al., 2018; Xu et al., 2019; Zak et al., 2019), processing in the olfactory bulb (Giraudet et al., 2002; Linster and Cleland, 2004; Tabor et al., 2004; Lin et al., 2006), and further normalization within piriform cortex, implemented by local inhibition. Inhibitory circuits within the piriform cortex have indeed been shown to play a major role in shaping piriform representations (Poo and Isaacson, 2009, 2011; Franks et al., 2011; Bolding and Franks, 2018).

Our findings complement recent studies describing normalization of piriform cortical responses to increasing concentrations (Bolding and Franks, 2017, 2018). Normalization of increasing concentrations is suggested to curtail responses to late activating glomeruli and thereby create concentration invariant representations due to a concentration invariant order of activation of receptors (Wilson et al., 2017; Chong et al., 2020). It is not clear how curtailing responses to late activating glomeruli may serve mixture coding. Adding odorants to a mixture is likely to change the order of activated glomeruli.

Most neurons in our data set were well fit by the normalization model, however, it is important to note that some neurons were not. These cells were mostly cells that did not increase their activity when mixture components were added, and it is possible that we only probed them with stimuli that push them to their saturated response levels. Although the quality of fit to the normalization model was not correlated with any electrophysiological signature (baseline firing, phase preference, and spike waveform), we cannot rule out the possibility that different neuronal populations integrate mixture components differently. Indeed principal neurons in the piriform cortex include subpopulations that differ in their localization across layers, biophysical properties, projection targets, and possibly tuning

width (Suzuki and Bekkers, 2006, 2011; Zhan and Luo, 2010; Diodato et al., 2016).

The finding that single piriform neurons may be sufficient to detect target odorants against background mixtures is in line with recently proposed models for target odorant detection from mixtures (Mathis et al., 2016; Singh et al., 2019). In these models, individual glomeruli are not informative about the presence of any specific odorant, but pooling information from a population of glomeruli, supports accurate classification. As piriform neurons receive inputs from multiple receptor channels, they are poised to be suitable for this classification. Importantly, however, these studies suggest that the synaptic connections between the olfactory bulb and piriform cortex must be learned for proper classification. Here we show that individual neurons perform this classification in naïve mice. Learning and synaptic plasticity may still improve classification accuracy as suggested by the models. Specific responses to mixture components have also been observed in the insect equivalent of the piriform cortex (but not in the antennal lobe) (Shen et al., 2013). Using linear classifiers, we showed that target odorant detection can be improved beyond what is achieved with single neurons by pooling inputs from a small population of neurons. Providing classifiers with temporal inputs yielded over-fitted models indicating that the anterior piriform cortex probably does not use a temporal code to represent odorants embedded in mixtures. This is in line with previous work indicating that the anterior piriform cortex primarily employs a rate code to project odor information (Miura et al., 2012; Haddad et al., 2013). The inputs for the classifiers were pseudo-populations pooled from multiple experiments. Pooling responses from multiple experiments removes noise-correlations and therefore is expected to improve classifier performance (Zohary et al., 1994). It should be noted, however, that previous measurements have found very little noise correlations in the piriform cortex during odor sampling (Miura et al., 2012).

In this study we recorded neuronal activity in anesthetized mice, however, signal to noise ratio of odor responses may be reduced in awake animals (Rinberg et al., 2006) and may also be modified during segmentation tasks either due to learning or to modulation by top-down inputs. It will therefore be interesting in the future to study how mixture coding and segmentation depend on the animal's state. Furthermore we focused on the ability to detect mixture components, yet, mixtures of odorants that are emitted from individual objects can create a unified percept in which the individual components are not identified (Jinks and Laing, 2001; Kadohisa and Wilson, 2006b; Barnes et al., 2008; Gottfried, 2010; Wilson and Sullivan, 2011; Howard and Gottfried, 2014). It will be interesting to investigate how normalization of mixture representations supports unified object percepts.

DATA AVAILABILITY STATEMENT

The raw data supporting the conclusions of this article will be made available by the authors, without undue reservation.

ETHICS STATEMENT

The animal study was reviewed and approved by the Hebrew University Ethics Committee.

AUTHOR CONTRIBUTIONS

SP and DR designed the study. SP and TL performed the experiments. SP, KH, and DR analyzed the data. All authors wrote and edited the manuscript.

FUNDING

ACKNOWLEDGMENTS

SUPPLEMENTARY MATERIAL

The Supplementary Material for this article can be found online at: https://www.frontiersin.org/articles/10.3389/fnsys.2020.604718/full#supplementary-material

Supplementary Figure 1 | Decoding analysis using sniff warped spike times. **(A)** Histogram of mean sniff duration all experiments. **(B)** Histogram of the coefficient of variation of sniff duration for all experiments. Dashed red line shows the median CV. **(C)** PSTH peak obtained in sniff aligned analysis vs. PSTH peak obtained in sniff warped analysis. Each dot represents one cell-stimulus pair. Dashed line is the unity line. **(D)** The area under the curve for each cell (with its best stimulus) as a function of the duration of response integration (in sniff cycles). Low performing cells (never reaching performance of 0.75) are shown in gray, high performing cells are shown in red. **(E)** The area under the curve using a sliding integration window of 0.8 π ($\sim$200 ms) as a function of the time of integration along the response (red) superimposed with the PSTH in response to the detected odorant (black). Twelve high performing neurons are shown. **(F)** Performance of linear classifiers as a function of the duration of the response integration window (in sniff cycles). **(G)** Performance of the classifiers as a function of temporal resolution (in sniff cycles).

REFERENCES

Abaffy, T., Matsunami, H., and Luetje, C. W. (2006). Functional analysis of a mammalian odorant receptor subfamily. *J. Neurochem.* 97, 1506–1518. doi: 10.1111/j.1471-4159.2006.03859.x

Ackels, T., Jordan, R., Schaefer, A. T., and Fukunaga, I. (2020). Respiration-locking of olfactory receptor and projection neurons in the mouse olfactory bulb and its modulation by brain state. *Front. Cell. Neurosci.* 14:220. doi: 10.3389/fncel.2020.00220

Araneda, R. C., Kini, A. D., and Firestein, S. (2000). The molecular receptive range of an odorant receptor. *Nat. Neurosci.* 3, 1248–1255. doi: 10.1038/81774

Arevian, A. C., Kapoor, V., and Urban, N. N. (2008). Activity-dependent gating of lateral inhibition in the mouse olfactory bulb. *Nat. Neurosci.* 11, 80–87. doi: 10.1038/nn2030

Aungst, J. L., Heyward, P. M., Puche, A. C., Karnup, S. V., Hayar, A., Szabo, G., et al. (2003). Centre–surround inhibition among olfactory bulb glomeruli. *Nature* 426, 623–629. doi: 10.1038/nature02185

Barnes, D. C., Hofacer, R. D., Zaman, A. R., Rennaker, R. L., and Wilson, D. A. (2008). Olfactory perceptual stability and discrimination. *Nat. Neurosci.* 11, 1378–1380. doi: 10.1038/nn.2217

Bolding, K. A., and Franks, K. M. (2017). Complementary codes for odor identity and intensity in olfactory cortex. *eLife* 6:e22630.

Bolding, K. A., and Franks, K. M. (2018). Recurrent cortical circuits implement concentration-invariant odor coding. *Science* 361:eaat6904. doi: 10.1126/science.aat6904

Brody, C. D., and Hopfield, J. J. (2003). Simple networks for spike-timing-based computation, with application to olfactory processing. *Neuron* 37, 843–852. doi: 10.1016/s0896-6273(03)00120-x

Brungart, D. S., Simpson, B. D., Ericson, M. A., and Scott, K. R. (2001). Informational and energetic masking effects in the perception of multiple simultaneous talkers. *J. Acoust. Soc. Am.* 110, 2527–2538. doi: 10.1121/1.1408946

Carandini, M., and Heeger, D. J. (2012). Normalization as a canonical neural computation. *Nat. Rev. Neurosci.* 13, 51–62. doi: 10.1038/nrn3136

Chong, E., Moroni, M., Wilson, C., Shoham, S., Panzeri, S., and Rinberg, D. (2020). Manipulating synthetic optogenetic odors reveals the coding logic of olfactory perception. *Science* 368:eaba2357. doi: 10.1126/science.aba2357

Davison, I. G., and Ehlers, M. D. (2011). Neural circuit mechanisms for pattern detection and feature combination in olfactory cortex. *Neuron* 70, 82–94. doi: 10.1016/j.neuron.2011.02.047

Diodato, A., Ruinart de Brimont, M., Yim, Y. S., Derian, N., Perrin, S., Pouch, J., et al. (2016). Molecular signatures of neural connectivity in the olfactory cortex. *Nat. Commun.* 7:12238.

Duchamp-Viret, P., Duchamp, A., and Chaput, M. A. (2003). Single olfactory sensory neurons simultaneously integrate the components of an odour mixture. *Eur. J. Neurosci.* 18, 2690–2696. doi: 10.1111/j.1460-9568.2003.03001.x

Erskine, A., Ackels, T., Dasgupta, D., Fukunaga, I., and Schaefer, A. T. (2019). Mammalian olfaction is a high temporal bandwidth sense. *bioRxiv* [Preprint]. doi: 10.1101/570689

Fantana, A. L., Soucy, E. R., and Meister, M. (2008). Rat olfactory bulb mitral cells receive sparse glomerular inputs. *Neuron* 59, 802–814. doi: 10.1016/j.neuron.2008.07.039

Franks, K. M., Russo, M. J., Sosulski, D. L., Mulligan, A. A., Siegelbaum, S. A., and Axel, R. (2011). Recurrent circuitry dynamically shapes the activation of piriform cortex. *Neuron* 72, 49–56. doi: 10.1016/j.neuron.2011.08.020

Ghosh, S., Larson, S. D., Hefzi, H., Marnoy, Z., Cutforth, T., Dokka, K., et al. (2011). Sensory maps in the olfactory cortex defined by long-range viral tracing of single neurons. *Nature* 472, 217–220. doi: 10.1038/nature09945

Giessel, A. J., and Datta, S. R. (2014). Olfactory maps, circuits and computations. *Curr. Opin. Neurobiol.* 0, 120–132. doi: 10.1016/j.conb.2013.09.010

Giraudet, P., Berthommier, F., and Chaput, M. (2002). Mitral cell temporal response patterns evoked by odor mixtures in the rat olfactory bulb. *J. Neurophysiol.* 88, 829–838. doi: 10.1152/jn.2002.88.2.829

Gottfried, J. A. (2010). Central mechanisms of odour object perception. *Nat. Rev. Neurosci.* 11, 628–641. doi: 10.1038/nrn2883

Grabska-Barwińska, A., Barthelmé, S., Beck, J., Mainen, Z. F., Pouget, A., and Latham, P. E. (2017). A probabilistic approach to demixing odors. *Nat. Neurosci.* 20, 98–106. doi: 10.1038/nn.4444

Green, D. M., and Swets, J. A. (1966). *Signal Detection Theory and Psychophysics*. New York: John Wiley & Sons, Inc.

Grosmaitre, X., Fuss, S. H., Lee, A. C., Adipietro, K. A., Matsunami, H., Mombaerts, P., et al. (2009). SR1, a mouse odorant receptor with an unusually broad response profile. *J. Neurosci.* 29, 14545–14552. doi: 10.1523/jneurosci.2752-09.2009

Grossman, K. J., Mallik, A. K., Ross, J., Kay, L. M., and Issa, N. P. (2008). Glomerular activation patterns and the perception of odor mixtures. *Eur. J. Neurosci.* 27, 2676–2685. doi: 10.1111/j.1460-9568.2008.06213.x

Haddad, R., Lanjuin, A., Madisen, L., Zeng, H., Murthy, V. N., and Uchida, N. (2013). Olfactory cortical neurons read out a relative time code in the olfactory bulb. *Nat. Neurosci.* 16, 949–957. doi: 10.1038/nn.3407

Hagiwara, A., Pal, S. K., Sato, T. F., Wienisch, M., and Murthy, V. N. (2012). Optophysiological analysis of associational circuits in the olfactory cortex. *Front. Neural Circuits* 6:18. doi: 10.3389/fncir.2012.00018

Hopfield, J. J. (1995). Pattern recognition computation using action potential timing for stimulus representation. *Nature* 376, 33–36. doi: 10.1038/376033a0

Howard, J. D., and Gottfried, J. A. (2014). Configural and elemental coding of natural odor mixture components in the human brain. *Neuron* 84, 857–869. doi: 10.1016/j.neuron.2014.10.012

Jinks, A., and Laing, D. G. (2001). The analysis of odor mixtures by humans: evidence for a configurational process. *Physiol. Behav.* 72, 51–63. doi: 10.1016/s0031-9384(00)00407-8

Kadohisa, M., and Wilson, D. A. (2006a). Olfactory cortical adaptation facilitates detection of odors against background. *J. Neurophysiol.* 95, 1888–1896. doi: 10.1152/jn.00812.2005

Kadohisa, M., and Wilson, D. A. (2006b). Separate encoding of identity and similarity of complex familiar odors in piriform cortex. *Proc. Natl. Acad. Sci. U.S.A.* 103, 15206–15211. doi: 10.1073/pnas.0604313103

Kajiya, K., Inaki, K., Tanaka, M., Haga, T., Kataoka, H., and Touhara, K. (2001). Molecular bases of odor discrimination: reconstitution of olfactory receptors that recognize overlapping sets of odorants. *J. Neurosci.* 21, 6018–6025. doi: 10.1523/jneurosci.21-16-06018.2001

Kurahashi, T., Lowe, G., and Gold, G. H. (1994). Suppression of odorant responses by odorants in olfactory receptor cells. *Science* 265, 118–120. doi: 10.1126/science.8016645

Lei, H., Mooney, R., and Katz, L. C. (2006). Synaptic integration of olfactory information in mouse anterior olfactory nucleus. *J. Neurosci.* 26, 12023–12032. doi: 10.1523/jneurosci.2598-06.2006

Li, Z., and Hertz, J. (2000). Odour recognition and segmentation by a model olfactory bulb and cortex. *Network* 11, 83–102. doi: 10.1088/0954-898x_11_1_305

Lin, D. Y., Shea, S. D., and Katz, L. C. (2006). Representation of natural stimuli in the rodent main olfactory bulb. *Neuron* 50, 937–949. doi: 10.1016/j.neuron.2006.03.021

Linster, C., and Cleland, T. A. (2004). Configurational and elemental odor mixture perception can arise from local inhibition. *J. Comput. Neurosci.* 16, 39–47. doi: 10.1023/b:jcns.0000004840.87570.2e

Linster, C., Henry, L., Kadohisa, M., and Wilson, D. A. (2007). Synaptic adaptation and odor-background segmentation. *Neurobiol. Learn. Mem.* 87, 352–360. doi: 10.1016/j.nlm.2006.09.011

Malnic, B., Hirono, J., Sato, T., and Buck, L. B. (1999). Combinatorial receptor codes for odors. *Cell* 96, 713–723. doi: 10.1016/s0092-8674(00)80581-4

Mathis, A., Rokni, D., Kapoor, V., Bethge, M., and Murthy, V. N. (2016). Reading out olfactory receptors: feedforward circuits detect odors in mixtures without demixing. *Neuron* 91, 1110–1123. doi: 10.1016/j.neuron.2016.08.007

McDermott, J. H. (2009). The cocktail party problem. *Curr. Biol.* 19, R1024–R1027.

McGann, J. P., Pírez, N., Gainey, M. A., Muratore, C., Elias, A. S., and Wachowiak, M. (2005). Odorant representations are modulated by intra- but not interglomerular presynaptic inhibition of olfactory sensory neurons. *Neuron* 48, 1039–1053. doi: 10.1016/j.neuron.2005.10.031

Miura, K., Mainen, Z. F., and Uchida, N. (2012). Odor representations in olfactory cortex: distributed rate coding and decorrelated population activity. *Neuron* 74, 1087–1098. doi: 10.1016/j.neuron.2012.04.021

Oka, Y., Omura, M., Kataoka, H., and Touhara, K. (2004). Olfactory receptor antagonism between odorants. *EMBO J.* 23, 120–126. doi: 10.1038/sj.emboj.7600032

Penker, S., Licht, T., Hofer, K. T., and Rokni, D. (2020). Reliable readout of mixture components from small populations of anterior piriform cortical neurons. *BioRxiv* [Preprint]. doi: 10.1101/2019.12.26.888693v4

Poo, C., and Isaacson, J. S. (2009). Odor representations in olfactory cortex: "sparse" coding, global inhibition, and oscillations. *Neuron* 62, 850–861. doi: 10.1016/j.neuron.2009.05.022

Poo, C., and Isaacson, J. S. (2011). A major role for intracortical circuits in the strength and tuning of odor-evoked excitation in olfactory cortex. *Neuron* 72, 41–48. doi: 10.1016/j.neuron.2011.08.015

Reddy, G., Zak, J. D., Vergassola, M., and Murthy, V. N. (2018). Antagonism in olfactory receptor neurons and its implications for the perception of odor mixtures. *eLife* 7:e34958.

Rinberg, D., Koulakov, A., and Gelperin, A. (2006). Sparse odor coding in awake behaving mice. *J. Neurosci.* 26, 8857–8865. doi: 10.1523/jneurosci.0884-06.2006

Rokni, D., Hemmelder, V., Kapoor, V., and Murthy, V. N. (2014). An olfactory cocktail party: figure-ground segregation of odorants in rodents. *Nat. Neurosci.* 17, 1225–1232. doi: 10.1038/nn.3775

Roland, B., Deneux, T., Franks, K. M., Bathellier, B., and Fleischmann, A. (2017). Odor identity coding by distributed ensembles of neurons in the mouse olfactory cortex. *eLife* 6:e26337.

Rubin, B. D., and Katz, L. C. (1999). Optical imaging of odorant representations in the mammalian olfactory bulb. *Neuron* 23, 499–511. doi: 10.1016/s0896-6273(00)80803-x

Shen, K., Tootoonian, S., and Laurent, G. (2013). Encoding of mixtures in a simple olfactory system. *Neuron* 80, 1246–1262. doi: 10.1016/j.neuron.2013.08.026

Shusterman, R., Smear, M. C., Koulakov, A. A., and Rinberg, D. (2011). Precise olfactory responses tile the sniff cycle. *Nat. Neurosci.* 14, 1039–1044. doi: 10.1038/nn.2877

Singh, V., Tchernookov, M., and Balasubramanian, V. (2019). What the odor is not: Estimation by elimination. *BioRxiv* [Preprint]. doi: 10.1101/568626v1

Sosulski, D. L., Bloom, M. L., Cutforth, T., Axel, R., and Datta, S. R. (2011). Distinct representations of olfactory information in different cortical centres. *Nature* 472, 213–216. doi: 10.1038/nature09868

Soucy, E. R., Albeanu, D. F., Fantana, A. L., Murthy, V. N., and Meister, M. (2009). Precision and diversity in an odor map on the olfactory bulb. *Nat. Neurosci.* 12, 210–220. doi: 10.1038/nn.2262

Stern, M., Bolding, K. A., Abbott, L., and Franks, K. M. (2018). A transformation from temporal to ensemble coding in a model of piriform cortex. *eLife* 7:e34831.

Stettler, D. D., and Axel, R. (2009). Representations of odor in the piriform cortex. *Neuron* 63, 854–864. doi: 10.1016/j.neuron.2009.09.005

Suzuki, N., and Bekkers, J. M. (2006). Neural coding by two classes of principal cells in the mouse piriform cortex. *J. Neurosci.* 26, 11938–11947. doi: 10.1523/jneurosci.3473-06.2006

Suzuki, N., and Bekkers, J. M. (2011). Two layers of synaptic processing by principal neurons in piriform cortex. *J. Neurosci.* 31, 2156–2166. doi: 10.1523/jneurosci.5430-10.2011

Suzuki, N., and Bekkers, J. M. (2012). Microcircuits mediating feedforward and feedback synaptic inhibition in the piriform cortex. *J. Neurosci.* 32, 919–931. doi: 10.1523/jneurosci.4112-11.2012

Szyszka, P., Stierle, J. S., Biergans, S., and Galizia, C. G. (2012). The speed of smell: odor-object segregation within milliseconds. *PLoS One* 7:e36096. doi: 10.1371/journal.pone.0036096

Tabor, R., Yaksi, E., Weislogel, J.-M., and Friedrich, R. W. (2004). Processing of odor mixtures in the zebrafish olfactory bulb. *J. Neurosci.* 24, 6611–6620. doi: 10.1523/jneurosci.1834-04.2004

Takeuchi, H., Ishida, H., Hikichi, S., and Kurahashi, T. (2009). Mechanism of olfactory masking in the sensory cilia. *J. Gen. Physiol.* 133, 583–601. doi: 10.1085/jgp.200810085

Urban, N. N. (2002). Lateral inhibition in the olfactory bulb and in olfaction. *Physiol. Behav.* 77, 607–612. doi: 10.1016/s0031-9384(02)00895-8

Vinograd, A., Livneh, Y., and Mizrahi, A. (2017). History-dependent odor processing in the mouse olfactory bulb. *J. Neurosci.* 37, 12018–12030. doi: 10.1523/jneurosci.0755-17.2017

Wilson, C. D., Serrano, G. O., Koulakov, A. A., and Rinberg, D. (2017). A primacy code for odor identity. *Nat. Commun.* 8:1477.

Wilson, D. A. (2003). Rapid, experience-induced enhancement in odorant discrimination by anterior piriform cortex neurons. *J. Neurophysiol.* 90, 65–72. doi: 10.1152/jn.00133.2003

Wilson, D. A., and Sullivan, R. M. (2011). Cortical processing of odor objects. *Neuron* 72, 506–519. doi: 10.1016/j.neuron.2011.10.027

Xu, L., Li, W., Voleti, V., Hillman, E. M. C., and Firestein, S. (2019). Widespread receptor driven modulation in peripheral olfactory coding. *bioRxiv* [Preprint] doi: 10.1101/760330v1

Xu, L., Li, W., Voleti, V., Zou, D.-J., Hillman, E. M. C., and Firestein, S. (2020). Widespread receptor-driven modulation in peripheral olfactory coding. *Science* 368:eaaz5390. doi: 10.1126/science.aaz5390

Yokoi, M., Mori, K., and Nakanishi, S. (1995). Refinement of odor molecule tuning by dendrodendritic synaptic inhibition in the olfactory bulb. *Proc. Natl. Acad. Sci. U.S.A.* 92, 3371–3375. doi: 10.1073/pnas.92.8.3371

Yoshida, I., and Mori, K. (2007). Odorant category profile selectivity of olfactory cortex neurons. *J. Neurosci.* 27, 9105–9114. doi: 10.1523/jneurosci.2720-07.2007

Zak, J. D., Gautam, R., Vergassola, M., and Murthy, V. N. (2019). Antagonistic odor interactions in olfactory sensory neurons are widespread in freely breathing mice. *bioRxiv* [Preprint]. Available online at: https://www.biorxiv.org/content/10.1101/847525v1.abstract (accessed December 15, 2019).

Zak, J. D., Reddy, G., Vergassola, M., and Murthy, V. N. (2020). Antagonistic odor interactions in olfactory sensory neurons are widespread in freely breathing mice. *Nat. Commun.* 11:3350.

Zhan, C., and Luo, M. (2010). Diverse patterns of odor representation by neurons in the anterior piriform cortex of awake mice. *J. Neurosci.* 30, 16662–16672. doi: 10.1523/jneurosci.4400-10.2010

Zohary, E., Shadlen, M. N., and Newsome, W. T. (1994). Correlated neuronal discharge rate and its implications for psychophysical performance. *Nature* 370, 140–143. doi: 10.1038/370140a0